Giant anisotropy of magnetocaloric effect in $TbMnO_3$ single crystals

Jin-Ling Jin, Xiang-Qun Zhang, Guo-Ke Li, and Zhao-Hua Cheng*
State Key Laboratory of Magnetism, Institute of Physics, Chinese Academy of Sciences, Beijing 100190, People's Republic of China

Lin Zheng and Yi Lu
Department of Physics, Baotou Normal University, Inner Mongolia Autonomous Regions, Baotou 014030, People's Republic of China
(Received 30 November 2010; published 27 May 2011)

The magnetocaloric effect (MCE) in $TbMnO_3$ single crystals was investigated by isothermal magnetization curves for the *ab* plane at low temperatures. Large magnetic entropy change, $\Delta S_M = -18.0$ J/kg K, and the refrigerant capacity, RC = 390.7 J/kg, are achieved near the ordering temperature of Tb^{3+} moment (T_N^{Tb}) under 70 kOe along the *a* axis. Furthermore, the $TbMnO_3$ single crystal exhibits a giant MCE anisotropy. The difference of ΔS_M and RC between the *a* and *b* axes is field and temperature dependent, which reaches maximum values of 11.4 J/kg K and 304.1 J/kg, respectively. By taking magnetocrystalline anisotropy into account, the rotating ΔS_M within the *ab* plane can be well simulated, indicating that the anisotropy of ΔS_M is directly contributed from the magnetocrystalline anisotropy. Our finding for giant MCE anisotropy in $TbMnO_3$ single crystals explores the possibility of using this material for magnetic refrigerators by rotating its magnetization vector rather than moving it in and out of the magnet.

DOI: 10.1103/PhysRevB.83.184431 PACS number(s): 75.30.Sg, 75.47.Lx, 75.30.Gw

I. INTRODUCTION

The magnetocaloric effect (MCE) describes the temperature change of magnetic materials in an adiabatic process caused by magnetic entropy change ΔS_M under external magnetic field. Materials with MCE may provide a better way for refrigeration due to such properties as cleanliness and high energy efficiency. To improve the efficiency of magnetic refrigeration, it requires magnetic refrigerant with a large magnetic entropy change. Giant magnetic entropy change around room temperature was obtained in materials with the first-order magnetic phase transition, such as the Gd-based alloys $Gd_5(Si_xGe_{1-x})_4$,[1] the Mn-based Ni-Mn-Ga alloys[2] and $MnFeP_{0.45}As_{0.55}$,[3] the Fe-based $LaFe_{13-x}(Al, Si)_x$,[4,5] as well as $(La_{1-x}M_x)MnO_3$ (M = Na, Ag, Ca, Sr, and Ba etc.).[6–10] Although numerous studies on MCE have been concentrated on exploring new materials with giant MCE near room temperature for domestic applications, large MCE in the low-temperature region from about 30 K down to sub-Kelvin temperatures is also essential for utilization in certain fields such as liquid hydrogen economy and space application.[11] Manganites may be promising candidates to satisfy this requirement because the transition temperature can be easily tuned by element substitution[12] or pressure.[13] $RMnO_3$ compounds with *R* as heavy rare-earth elements show low magnetic phase transition temperatures as the ionic radius of *R* decreases.[14]

Although the relationship between the magnetic phase transition and MCE is well known, the contribution from magnetocrystalline anisotropy (MCA) has not been sufficiently investigated. For most magnetic materials, the contribution from MCA to MCE at Curie temperatures is considerably lower than that from the paramagnetic-ferromagnetic phase transition. However, in the region of the spin-reorientation transition, the anisotropic and rotating MCE can be quite large. The contribution from the magnetization vector rotation to the total MCE is known to be higher for materials with high values of derivatives of the MCA with respect to temperature.[15] In the case of orthorhombic perovskite $TbMnO_3$ single crystals, Mn^{3+} moments go through incommensurate antiferromagnetic (AFM) order below $T_N \sim 42$ K and spiral magnetic order below $T_S \sim 27$ K, respectively. The magnetic spiral structure lies in the *bc* plane with the propagating vector along the *b* direction. This magnetic modulation can be switched to the *ab* plane by external magnetic field along the *a* or *b* direction.[16] The spiral magnetic structure results in multiferroic properties.[17] However, the effect of this special magnetic structure on MCE is not well understood yet. In this work, we present a study of the MCE in $TbMnO_3$ single crystal near the ordering temperature of Tb^{3+} moment (T_N^{Tb}) with magnetic field along both *a* and *b* axes. The reason for choosing $TbMnO_3$ single crystals is twofold. First, as the temperature is lowered, ordering of Tb^{3+} moments emerges accompanying the complex interplay between Tb^{3+} and Mn^{3+}.[18] This transition causes a considerable increase in magnetization, and, consequently, a large ΔS_M at low temperatures is expected. Magnetic interplay between Tb^{3+} and Mn^{3+} moments is observed below T_N^{Tb}. As Tb^{3+} moments can be easily aligned along external magnetic field, a small magnetic field is needed to induce reorientation of Mn^{3+} moments, which also contributes to the magnetic entropy change. Second, due to the large MCA of $TbMnO_3$ single crystal, large MCE anisotropy and rotating MCE are expected in $TbMnO_3$ single crystals. The MCE anisotropy can facilitate magnetic refrigeration through simply rotating the sample instead of moving it in and out of the magnet.

II. EXPERIMENTAL

A $TbMnO_3$ single crystal was grown by use of the floating zone method with four ellipsoidal mirrors (Crystal Systems Inc., FZ-T-10000-H-VI-VP). Powder x-ray diffraction confirmed that the sample was single phase and showed *Pbnm* symmetry. Back-reflection Laue x-ray diffraction experiment was carried out to check the single crystallinity and determine

the crystallographic direction. Magnetization measurements were performed on a commercial superconducting quantum interference device (SQUID) magnetometer (Quantum design, MPMS-XL).

III. RESULTS AND DISCUSSIONS

The thermal magnetization curves for a and b axes were plotted in Figs. 1(a) and 1(b), respectively. The measurements were carried out under a magnetic field of 1 kOe after zero field cooling (ZFC) and field cooling (FC) processes, respectively. With decreasing temperatures, a large increase in magnetization can be seen clearly. The kink point at 9 K indicated by the arrows in Fig. 1 corresponds to the ordering of Tb^{3+} moments (T_N^{Tb}). From the thermal magnetization curves, AFM ordering of Mn^{3+} moments at $T_N \sim 42$ K and spiral magnetic order at $T_S \sim 27$ K cannot be observed in these two directions. In order to see the nature of the transition clearly, temperature dependence of $1/M$ is plotted in the inset of Figs. 1(a) and 1(b). By fitting the experimental data above 100 K with the Curie-Weiss law, we get the effective magnetic moment $\mu_{\text{eff}} = 10.7\mu_B$ and $11.9\mu_B$, and Curie-Weiss temperature, $\theta_p = 20$ K and -60 K for the a and b axes, respectively. The effective magnetic moment is contributed by both Tb^{3+} with $9.5\mu_B$ and Mn^{3+} with $4.9\mu_B$. The considerably large difference between μ_{eff} and θ_p for the a and b axes indicates significant magnetic anisotropy between the two directions.

Full M versus H loops for each temperature were measured near T_N^{Tb} from 2 K to 40 K with an increment of 2 K through increasing magnetic field H from 0 to 70 kOe and then decreasing down to 0 kOe. The representative isothermal magnetization curves along the a and b axes with a magnetic field up to 70 kOe were plotted in Figs. 2(a) and 2(b), respectively. Almost no hysteresis loops can be observed from the isothermal magnetization curves except those at 2 K and 4 K for the b axis, which can be seen clearly in the inset of Fig. 2(b). The a-axis magnetization curves below T_N^{Tb}(9 K) show a sharp step in magnetization around 14 kOe

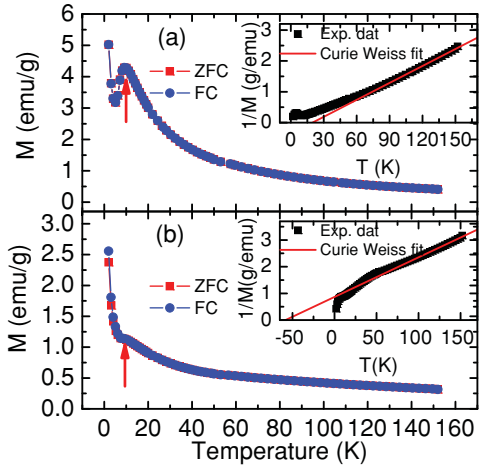

FIG. 1. (Color online) Thermal magnetization curves under FC and ZFC processes for (a) the a axis and (b) the b axis. The inset shows the relation of 1 M with temperature and the corresponding Curie-Weiss fitting curves.

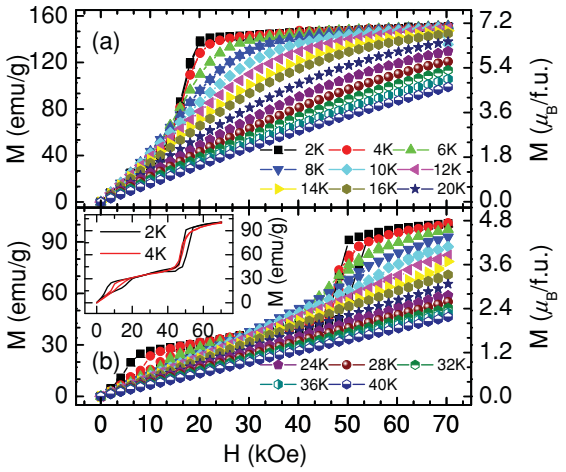

FIG. 2. (Color online) Representative magnetization isothermals at various temperatures for (a) the a axis and (b) the b axis. Both increasing and decreasing field measurement processes are included for each temperature. The curves at 2K and 4K for the b axis are shown in the inset of (b) for clarity.

and subsequently approach saturation magnetization up to $7.1\mu_B$/f.u. (formula unit) at 2 K. This step corresponds to a switch of the spin spiral modulation from the bc plane to the ac plane, which is induced by an external magnetic field. However, the two steps appear in the isothermal magnetization curves along the b axis below T_N^{Tb}. The first step around 8 kOe is induced by a small change in the magnetic modulation vector. The second step occurs at 48 kOe due to the switch of the spiral magnetic plane as in the case of a axis.[19,20] It approaches saturation but with a much smaller value of $4.7\mu_B$/f.u.at 2 K, suggesting a strong antiferromagnetic interaction along the b axis ($\theta_p = -60$ K).

The magnetic entropy change ΔS_M produced by the variation of external magnetic field from 0 to H can be calculated from the following equation:

$$\Delta S_M(T,H) = S_M(T,H) - S_M(T,0) = \int_0^H \left(\frac{\partial S}{\partial H}\right)_T dH. \tag{1}$$

By using the Maxwell's relation:

$$\left(\frac{\partial S}{\partial H}\right)_T = \left(\frac{\partial M}{\partial T}\right)_H. \tag{2}$$

One can obtain the following expression:

$$\Delta S_M(T,H) = \int_0^H \left(\frac{\partial M}{\partial T}\right)_H dH. \tag{3}$$

The magnetic entropy change ΔS_M can be calculated from magnetization isothermals by Eq. (3). Figures 3(a) and 3(b) show ΔS_M as a function of temperature under an external magnetic field from 0 to 70 kOe along the a and b axes, respectively. In the temperature region of 3-5 K, positive values of ΔS_M were observed for certain fields, which are more evident along the b axis. The positive magnetic entropy change at low temperatures is directly related to the magnetic spiral structure lies in the bc plane with the propagating vector along the b direction. Below T_N^{Tb}(9 K), the strong antiferromagnetic

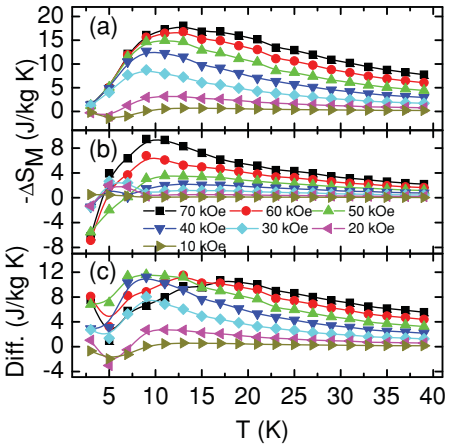

FIG. 3. (Color online) Magnetic entropy change versus temperature in various magnetic fields for (a) the a axis and (b) the b axis and (c) demonstrates the corresponding difference in ΔS_M between the a and b axes versus temperature.

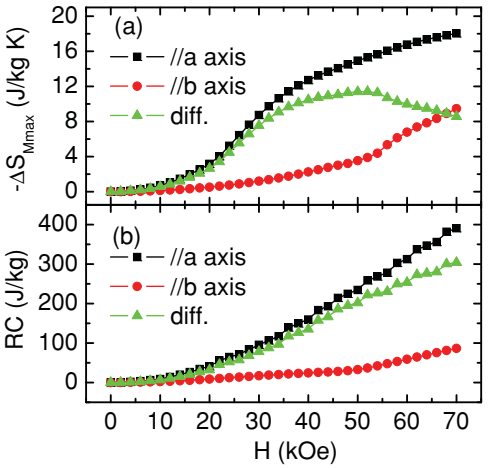

FIG. 4. (Color online) (a) Maximum and (b) RC for the a and b axes as well as the difference between the two axes.

coupling along b axis results in an antiferromagnetic ordering between Tb^{3+} and Mn^{3+} ions. An applied magnetic field will destroy the antiferromagnetic ordering and, consequently, induce a positive magnetic entropy change.[21] Due to the easy magnetization of a axis, a small field can induce the AFM-FM transition. Therefore, the positive magnetic entropy change occurs only at low fields. If the magnetic field is higher than 20 kOe, the magnetic ordering will be induced to ferromagnetic one, and, consequently, the magnetic entropy change becomes negative. On the other hand, the AFM state is much more robust for the b axis and the positive magnetic entropy change persists until 70 kOe. Noticeably, the spiral magnetic structure of Tb^{3+} and Mn^{3+} ions brings new features for the $TbMnO_3$ single crystal. This spiral magnetic structure makes the AFM-FM transition much easier for Tb^{3+} in $TbMnO_3$ than those with linear magnetic structures at low temperatures.[22] The metamagnetic-like transition further induces the spin reorientation of Mn^{3+} moment.[18] Consequently, small magnetic field can induce large ΔS_M in $TbMnO_3$ single crystal due to the combination of the above two transitions. Although the metamagnetic-like transitions occur, the hysteresis loss can be ignored from the full M versus H loops except that at 2 and 4 K for b axis. The reversible magnetic entropy change makes $TbMnO_3$ suitable for magnetic refrigeration at low temperatures.

For both directions, ΔS_M shows a broad peak in the vicinity of T_N^{Tb} and the peak broadens asymmetrically toward the higher-temperature region. The maximum value of ΔS_M under 70 kOe reaches -18.0 J/kg K for the a axis. By comparing with $HoMnO_3$ single crystal with similar magnetic transitions, it was found that the maximum value of ΔS_M under 70 kOe for $TbMnO_3$ single crystal along a axes is larger than that of $HoMnO_3$ (-13.1 J/kg K) near the transition temperature of Ho^{3+} although the magnetic moment of Tb^{3+} ($9.5\mu_B$) is smaller than Ho^{3+} ($10.5\mu_B$).[23]

By comparing ΔS_M for the a and b directions, a giant anisotropy of ΔS_M was observed in $TbMnO_3$ single crystal. Figures 3(c) shows the difference of ΔS_M between the a and b directions as a function of temperature under different magnetic fields. The corresponding difference of the peak values between the two directions is dependent on external magnetic field and reaches maximum of 11.4 J/kg K around 52 kOe [Fig. 4(a)].

It is proved that the refrigerant capacity, RC, is related not only to the magnitude but also to the peak width of ΔS_M. RC can be obtained by numerically integrating the area under the ΔS_M versus T curves, using the temperatures at half-maximum of the ΔS_M peak as the integration limits, suggested by Gschneidner *et al.*[24] Figure 4(b) demonstrates the values of RC as a function of applied field along the a and b axes. Although the difference of ΔS_M between the a and b axes reaches a maximum under the magnetic field of 52 kOe, the difference in RC increases monotonously with increasing magnetic field. The $TbMnO_3$ single crystal shows a larger refrigeration capacity along the a axis (390.7 J/kg) than along the b axis (86.7 J/kg) under 70 kOe.

In order to further investigate the origin of MCE anisotropy of the $TbMnO_3$ single crystal, the magnetization curves were measured by rotating the sample from the a to the b axis. The representative magnetization versus angle curves are shown

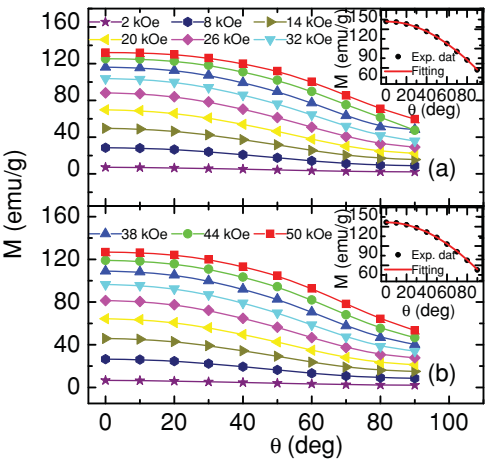

FIG. 5. (Color online) Representative rotating magnetization curves for (a) 14 K and (b) 16 K. The inset of (a) and (b) shows the fitting result for the curves under 50 kOe.

in Figs. 5(a) and 5(b) for 14 K and 16 K, respectively, which were acquired by rotating the sample from the a axis (0°) to the b axis (90°) with an increment of 10°. It is difficult to describe magnetocrystalline anisotropy energy for $TbMnO_3$ single crystal because of its complex magnetic structure with both Tb^{3+} and Mn^{3+} as magnetic ions. Based on the angle dependence of magnetization (Fig. 5), we can simply assume a uniaxial magnetocrystalline anisotropy for $TbMnO_3$ with the crystallographic direction a as the easy axis. The energy of the system can be written as:

$$\begin{aligned} E &= E_K + E_H \\ &= K_1 \sin^2\alpha + K_2 \sin^4\alpha - M_S H \cos(\theta - \alpha), \end{aligned} \quad (4)$$

where K_1 and K_2 are the second- and fourth-order magnetocrystalline anisotropy constants. $\theta$is the angle between the a axis and the magnetic field, and α is the angle between the a axis and the magnetization vector. The saturation magnetization M_S can be obtained from magnetization curve at high fields along the a axis. We can get the direction of the magnetization vector by minimizing the energy in Eq. (4) and calculate its value under each field. The fitting result of rotated magnetization under 50 kOe as a function of angle matches well the experimental data [inset of Figs. 5(a) and 5(b)].

The magnetocrystalline anisotropy constants can be obtained from magnetization curves along the hard magnetization axis, i.e., $\theta = 90°$. In the case of $\theta = 90°$, by minimizing the total energy, $\frac{\partial E}{\partial \alpha} = 0$, we obtain the relationship between magnetization M and magnetic field H along hard axis as follows:

$$H = \frac{2K_1}{M_S^2} M + \frac{4K_2}{M_S^4} M^3, \quad (5)$$

As shown in Fig. 6, a linear relationship between the magnetization M and the magnetic field H along hard axis implies that the contribution of the fourth-order magnetocrystalline anisotropy constant K_2 can be neglected. For simplicity, we just take K_1 into account. By fitting the magnetization curves along the hard b axis, we got $K_1 = 5.77 \times 10^7$ erg/cm^3 and 5.74×10^7 erg/cm^3 at 14 K and 16 K, respectively.

The contribution of magnetocrystalline anisotropy to rotating MCE under adiabatic magnetization of a single crystal can be written as follows:

$$\begin{aligned} \Delta S_M^R(H,\theta,K_1) &= \Delta S_M(\theta) - \Delta S_M(90°) \\ &= \int_{90°}^{\theta} \frac{dE_K(H,\theta,K_1)}{T} \\ &= K_1 \times \frac{\sin^2\alpha(H,\theta) - \sin^2\alpha(H,90°)}{T}, \end{aligned} \quad (6)$$

where α can be got by minimizing the energy in Eq. (4). We use the average magnetocrystalline anisotropy constant of 14 K and 16 K as that for 15 K. The calculated results demonstrate that $\Delta S_M^R(\theta)$ gradually decreases while rotating the sample from the a to the b axis under the magnetic field Fig. 7. The good consistence between the calculated results (red line) and the experimental data obtained from the isothermal magnetization curves (black dots) supports that the giant anisotropy of the magnetocaloric effect in the $TbMnO_3$ single crystal is directly related to its magnetocrystalline anisotropy.

The giant MCE anisotropy of the $TbMnO_3$ single crystal at low temperatures is largely due to Tb^{3+} ions. The ions of Tb^{3+} have large angular momentum that is not quenched by the crystal electric field because of shielding from 5s and 5p electrons. The 4f orbital assumes a preferred orientation along the magnetic moment as a result of the spin-orbital coupling, which results in a large magnetocrystalline magnetic anisotropy and giant anisotropy in ΔS_Mas a result. Knowing the heat capacity of the $TbMnO_3$ single crystal, $C_p \approx 5$J/mole K,[16] and its magnetic entropy change ΔS_M, we can estimate the adiabatic temperature change ΔT_{ad} by the following relation:

$$\Delta T_{ad} = -\frac{T}{C_P} \Delta S_M^R. \quad (7)$$

The maximum adiabatic temperature change of $\Delta T_{ad} \approx 6$ K can be achieved when the single crystal is rotated by 90° from the b to the a axis under a magnetic field of 50 kOe (Fig. 7). In addition to the traditional magnetic refrigerators via an order-disorder magnetic phase transition, our experimental

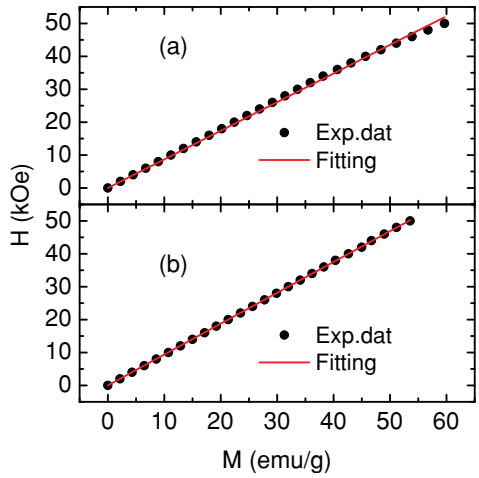

FIG. 6. (Color online) The function of magnetization versus magnetic field for (a) 14 K and (b) 16 K. Both the experimental data (black dotted line) and the fitting data (red line) are shown.

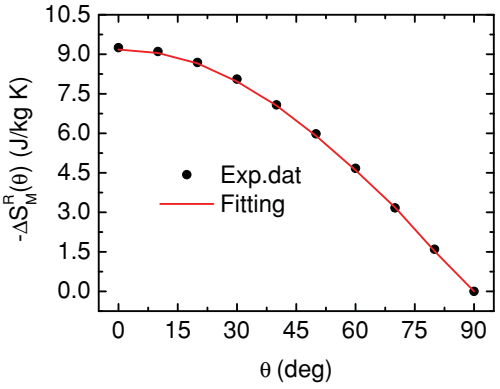

FIG. 7. (Color online) Rotating $\Delta S_M^R(\theta)$ as a function of rotating angle θ with the b axis as the starting direction under 50 kOe. Experimental data and calculated results are shown in the black dots and red line, respectively.

and theoretical results in anisotropy of MCE provide an alternative way for using the rotating MCE in magnetic refrigerators.

IV. Summary

A $TbMnO_3$ single crystal shows significant anisotropy in peak ΔS_M and RC, which reach 11.4 J/kg K and 304.1 J/kg, respectively. This anisotropy can be well fitted using uniaxial magnetocrystalline anisotropy. The giant MCE anisotropy in $TbMnO_3$ single crystal suggests that it can be used as a candidate for magnetic refrigerants at low temperatures by rotating it in a magnetic field, which is easier than moving it in and out of the magnet. Although the major investigations on MCE are focusing on the contribution of the exchange energy change during the order-disorder magnetic phase transition, the studies of MCE anisotropy in $TbMnO_3$ can open new arena in developing magnetic refrigerators.

ACKNOWLEDGMENTS

This work was supported by the National Basic Research Program of China (973 program, Grants No. 2009CB929201, No. 2010CB934202, and No. 2011CB921801) and the National Natural Sciences Foundation of China (50831006, 50931006, 51021061, and 11034004).

*Corresponding author: zhcheng@aphy.iphy.ac.cn

[1] V. K. Pecharsky and K. A. Gschneidner Jr., Phys. Rev. Lett. **78**, 4494 (1997).
[2] Y. Long, Z. Y. Zhang, and D. Wen, J. Appl. Phys. **98**, 046102 (2005).
[3] O. Tegus, E. Bruck, K. H. J. Buschow, and F. R. de Boer, Nature **415**, 150 (2002).
[4] A. Fujita, S. Koiwai, S. Fujieda, K. Fukamichi, T. Kobayashi, H. Tsuji, S. Kaji, and A. T. Saito, J. Appl. Phys. **105**, 07A936 (2009).
[5] B. G. Shen, J. R. Sun, F. X. Hu, H. W. Zhang, and Z. H. Cheng, Adv. Mater. **21**, 4545 (2009)
[6] W. Chen, W. Zhong, D. L. Hou, R. W. Gao, W. C. Feng, M. G. Zhu, and Y. W. Du, J. Phys. Condens. Matter **14**, 11889 (2002).
[7] T. Tang, K. M. Gu, Q. Q. Gao, D. H. Wang, S. Y. Zhang, and Y. W. Du, J. Magn. Magn. Mater. **222**, 110 (2000).
[8] M. H. Phan, S. C. Yu, and N. H. Hur, J. Magn. Magn. Mater. **262**, 407 (2003).
[9] R. V. Demin, L. I. Koroleva, Phys. Solid State **46**, 1081 (2004).
[10] M. H. Phan, S. B. Tian, D. Q. Hoang, S. C. Yu, C. Nguyen, and A. N. Ulyanov, J. Magn. Magn. Mater. **258**, 309 (2003).
[11] K. A. Gschneidner, V. K. Pecharsky, and A. O. Tsoko, Rep. Prog. Phys. **68**, 1479 (2005).
[12] R. Venkatesh, K. Sethupathi, M. Pattabiraman, and G. Rangarajan, J. Magn. Magn. Mater. **310**, 2813 (2007).
[13] Y. Sun, J. Kamarad, Z. Arnold, Z. Q. Kou, and Z. H. Cheng, Appl. Phys. Lett. **88**, 102505 (2006).
[14] T. Kimura, S. Ishihara, H. Shintani, T. Arima, K. T. Takahashi, K. Ishizaka, and Y. Tokura, Phys. Rev. B **68**, 060403(R) (2003).
[15] S. A. Nikitin, K. P. Skokov, Y. S. Koshkid'ko, Y. G. Pastushenkov, and T. I. Ivanova, Phys. Rev. Lett. **105**, 137205 (2010).
[16] T. Kimura, T. Goto, H. Shintani, K. Ishizaka, T. Arima, and Y. Tokura, Nature **426**, 58 (2003).
[17] T. Kimura, Annu. Rev. Mater. Res. **37**, 387 (2007).
[18] N. Aliouane *et al.* , J. Phys. Condens. Matter **20**, 434215 (2008).
[19] D. Meier, N. Aliouane, D. N. Argyriou, J. A. Mydosh, and T. Lorenz, New J. Phys. **9**, 100 (2007).
[20] A. Pimenov, A. Shuvaev, A. Loidl, F. Schrettle, A. A. Mukhin, V. D. Travkin, V.Yu. Ivanov, and A. M. Balbashov, Phys. Rev. Lett. **102**, 107203 (2009).
[21] T. Krenke, E. Duman, M. Acet, E. F. Wassermann, X. Moya, L. Manosa, and A. Planes, Nat. Mater. **4**, 450 (2005).
[22] N. Biškup, A. de Andrés, and M. García Hernández, Phys. Rev. B **78**, 184435 (2008).
[23] A. Midya, P. Manda, S. Das, S. Banerjee, L. S. Sharath Chandra, V. Ganesan, and S. Roy Barman, Appl. Phys. Lett. **96**, 142514 (2010).
[24] K. A. Gschneidner Jr., V. K. Pecharsky, A. O. Pecharsky, and C. B. Zimm, Mater. Sci. Forum **315-317**, 69 (1999).